THE OBSERVABILITY OF SECONDARY DOPPLER PEAKS

Michael P. Hobson
Mullard Radio Astronomy Observatory, Cambridge, UK.

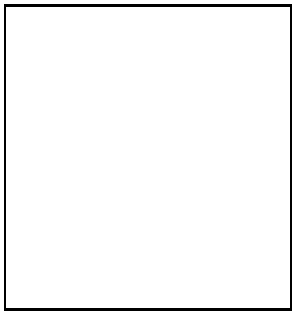

Abstract

By proposing a statistic for the detection of secondary (Doppler) peaks in the CMBR power spectrum, the significance level at which such peaks may be detected are computed for a large range of model CMBR experiments. In particular, we investigate experimental design features required to distinguish between competing cosmological theories, such as cosmic strings and inflation, by establishing whether or not secondary peaks are present in the CMBR power spectrum.

1 Introduction

Experimental measurement of the Doppler peaks' positions and heights would fix at least some combinations of cosmological parameters (e.g. H_0, Ω_0 etc.) which are left free in inflationary models [1]. Furthermore, as shown by [2, 3], the *absence* of secondary Doppler peaks is a robust prediction for cosmic strings, although this may or may not be the case for textures [4, 5]. Therefore it appears that even determining whether or not there are secondary Doppler peaks offers an important alternative motivation for measuring the CMBR power spectrum.

We address this issue by proposing a statistic for detecting secondary oscillations, and studying how it performs for various models, using different experimental strategies. The results are encoded in a detection function Σ which indicates to within how many sigmas we can claim a detection of secondary oscillations, given a particular model and experiment.

We apply the statistic to both the standard CDM scenario and an open CDM model which is tuned to confuse inflation and cosmic strings in all but the existence or otherwise of secondary oscillations. For a wide range of experiments we allow the beam size, sky coverage, and detector noise to vary, and use this framework to compute the detection function for secondary peaks.

2 Power spectrum estimation from real observations

There are several factors affecting how well one can measure the CMBR power spectrum from real observations, which we now discuss.

(i) Distortion of the underlying spectrum due to the finite size of the observed field. For (square) fields of size $L \geq 4$ degrees (suitably windowed with a cosine bell or Hann window) this is not a severe problem for detecting secondary peak structure.

(ii) Cosmic/sample variance, which places constraints on the minimum sky-coverage necessary to achieve a given accuracy. Roughly speaking, if $f_{\rm s}$ is the fraction of sky observed, then $\sigma^2(C_\ell)/C_\ell^2 \approx 1/(\ell f_{\rm s})$.

(iii) Instrumental noise, which we shall assume is uncorrelated for simplicity, and characterised by $\sigma_{\rm pix}$, the rms pixel noise, and $\Omega_{\rm pix}$, the area of a pixel. If we consider the most general case where only a fraction $f_{\rm s}$ of the sky is mapped, then for a detector of fixed sensitivity, and for a fixed total observing time, then by varying $\Omega_{\rm pix}$ and $f_{\rm s}$ the quantity $w^{-1} = \sigma_{\rm pix}^2 \Omega_{\rm pix}(4\pi/f_{\rm s})$, remains constant, and is therefore an important qualifier for noise on maps obtained using different scanning strategies.

(iv) Diffuse foreground emission, which can severely hamper the measurement of CMBR anisotropies. A discussion of these foreground components, and the regions of frequency/multipole space in which each dominates, is given by [6]. The main components of this foreground are Galactic dust, synchrotron and free-free emission. Algorithms for separating these components from the CMBR signal are discussed by [6] and [7]. Typically the errors associated with the separation process are of a similar magnitude to the average errors on an individual frequency channel due to instrumental noise alone, but details depend on the separation algorithm used.

(v) Point sources, which cannot be removed from spectral information alone. This requires the identification of the sources by higher-resolution observations at a frequency close to that of the CMBR observations, with sufficient flux sensitivity to indentify all point sources down to some flux limit roughly equal to the instrumental noise of the CMBR observations. We note here that although it is generally believed that point source contamination becomes less important as the observing frequency increases above about 100 GHz, there is no direct evidence for this. Moreover, even the population of radio point sources at frequencies above about 10 GHz is rather uncertain, and it may be inadvisable to rely on low frequency surveys such as the 1.5 GHz VLA FIRST survey [8] to subtract point sources from CMBR maps made at much higher frequencies.

3 Observing Doppler peaks in standard CDM

The idea is to apply to a particular model a statistic sensitive only to the existence or absence of secondary oscillations in the power spectrum. In this section we consider the power spectrum predicted by the standard inflation/CDM scenario with $\Omega_0 = 1$, $h_0 = 0.5$ and $\Omega_b = 0.05$ (which we shall call sCDM).

To this end we first compute the average broad band power C_i in each of several equally spaced-bins, denoted by horizontal bars in Fig. 1. We then infer the convexity $\mathcal{C}_i$ of the spectrum at each bin position (apart from the first and last bins) from $\mathcal{C}_i = (C_{i-1} + C_{i+1})/2 - C_i$. These convexities are all negative if there are no secondary peaks, but alternate in sign for sCDM. If the overall error in $\mathcal{C}_i$ is $\sigma^2(\mathcal{C}_i)$ then one can define an oscillation detection function as

$$\Sigma_i = \frac{|\langle \mathcal{C}_i \rangle|}{\sigma(\mathcal{C}_i)}, \tag{1}$$

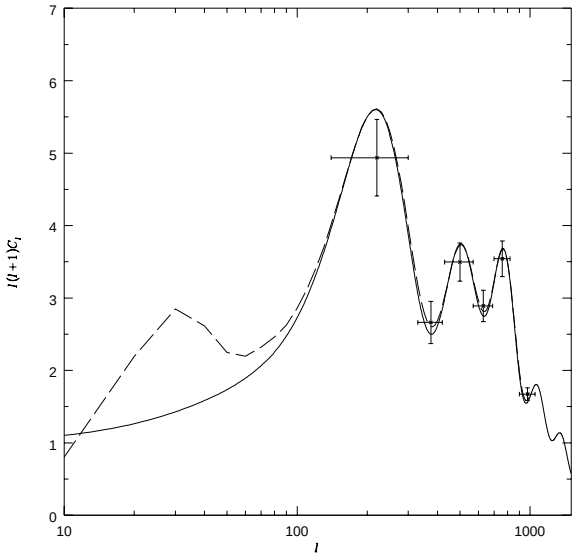

Figure 1: The ensemble average power spectrum predicted by sCDM (solid line), and the ensemble average power spectrum for a square observing field of size 10 degrees after windowing with a cosine bell (dashed line). The points indicate the corresponding power spectrum estimates for a particular realisation in each of the bins indicated by the horizontal error bars. The vertical error bars indicate the theoretical cosmic/sample variance in the absence of noise.

for $i = 2$ and $i = 4$, which tells us to within how many sigmas we can claim a detection of secondary peaks. The method for computing the estimates C_i of the power spectrum in each bin, and their associated standard errors, taking into account limited sky-coverage and instrumental noise, are discussed in detail in [9] and [10].

From Fig. 1 we see that the first dip in the sCDM power spectrum is more easily detected than than the second one, a situation only exacerbated by finite resolution and the presence of instrumental noise. Therefore we shall confine ourselves to considering the detection function Σ_2, which from now on we refer to simply as Σ.

The detection function $\Sigma = \Sigma(L, \theta_b, w^{-1})$, where L is the linear size of the observed (square) field [the all-sky limit can be recovered by setting $L^2 = 4\pi$ sr $\approx (202 \text{ deg})^2$], θ_b is FWHM of the observing beam, and w^{-1} is the noise level discussed above. This function is plotted in Fig. 2 for the low noise case $w^{-1} = (25\mu\text{K})^2(\text{deg})^2$ and the high-noise case $w^{-1} = (60\mu\text{K})^2(\text{deg})^2$.

For any beamsize there is a maximum sky coverage beyond which the detection is not improved. If anything the level of the detection decreases, but typically not by much. The ideal scanning strategy is then defined by a line $L_i(\theta_b)$ which intersects the contours of Σ at the lowest L-value at which a plateau has been achieved in the detection function. The significance of the detection obtained for an ideally scanned experiment depends on the beam size. For example, in the low-noise case, if $\theta_b = 0.6^\circ$, the ideal coverage is a patch of $L_i(0.6^\circ) = 5$ degrees, which results in a 3-sigma detection. If $\theta_b = 0.5^\circ$, on the other hand, an 8-sigma detection can be obtained with $L_i = 35$ degrees. The detection provided by an optimally scanned experiment increases at first very quickly as the beam is reduced below $\theta_b = 0.6^\circ$ (from 3-sigma at $\theta = 0.6^\circ$ to 33-sigma at $\theta_b = 0.2^\circ$). By reducing θ_b from 0.2° to zero, however, the detection is only increased by 2-sigma (from 33 to 35). For this level of noise the maximal detection is 35 sigma and is achieved with $\theta_b < 3'$ and all-sky coverage. For low noise levels all-sky coverage is never harmful, but it is the beamsize that determines how good a detection can be achieved, and how much sky coverage is actually required for an optimum level of detection.

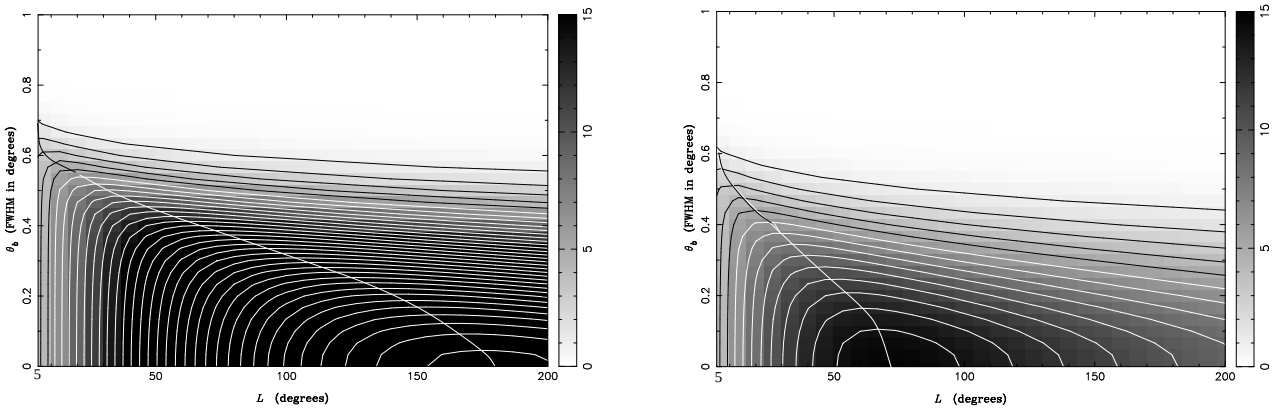

Figure 2: (Left) Low noise $w^{-1} = (25\mu K)^2(\text{deg})^2$ contours of the Σ function. Sky coverage L varies between 5 degrees and all sky ($L = 202$ degrees), and the beamsize FWHM between 0 and 1 degrees. (Right) High noise $w^{-1} = (60\mu K)^2(\text{deg})^2$ contours of the Σ function.

For noise levels of the order $w^{-1} = (25\mu K)^2(\text{deg})^2$ the overall picture is always as in Fig. 2. In particular, there is always a top contour indicating the maximal detection allowed by the given noise level. The maximum Σ is always achieved with infinite resolution, but one falls short of this maximum by only a couple of sigmas if $\theta_b \approx 0.1^\circ$. If the noise is much smaller than this, however, the summit of Σ is beyond $L = 202^\circ$. For $w^{-1} = (15\mu K)^2(\text{deg})^2$, for instance, all-sky coverage becomes ideal for any $\theta_b < 0.3^\circ$.

If, on the other hand, the noise is much larger than $w^{-1} = (25\mu K)^2(\text{deg})^2$ then the Σ contours are qualitatively different, as shown in Fig. 2 for $w^{-1} = (60\mu K)^2(\text{deg})^2$. The beamsize is now a crucial factor. A beamsize of $\theta_b = 0.5^\circ$ would provide a 3-sigma detection (with $L_i = 10^\circ$), but reducing the beamsize to about $\theta_b = 0.4^\circ$ improves the detection to 6-sigma (with $L_i = 20^\circ$). It is also clear from the figure that, for high noise levels, forcing all-sky coverage dramatically decreases the detection.

4 Open CDM models and cosmic strings

We may repeat the above analysis for different cosmological models. We therefore consider the case of maximal confusion between inflation/CDM and cosmic string scenarios by comparing a cosmic strings model with a CDM model for which the main peak in the power spectrum has the same position and shape (but the latter exhibits secondary peaks). For definiteness we have chosen a CDM theory with a flat primordial spectrum, $\Omega_0 = 0.3$, $h_0 = 0.6$, and $\Omega_b h_0^2 = 0.02$. We shall call this theory stCDM, the CDM competitor of cosmic strings. As before we simply study the first dip detection function of stCDM, and then take this detection function as a cosmic string rejection function.

In Fig. 3 we show the angular power spectrum of stCDM (solid line) and a possible power spectrum for cosmic strings (dotted line). We then simply repeat the same exercise as in the previous section to obtain the detection function of the first dip of stCDM. The results are shown in Fig. 4 for the same noise levels as before.

Overall we see that in signal dominated regions the detection is much better for stCDM than for sCDM. This is because features at higher ℓ have a smaller cosmic/sample variance (which is proportional to $1/\ell$). It can be checked that the cosmic/sample variance limit, obtained with a single-dish experiment with no noise, is now $\Sigma \approx 197L^2/(4\pi)$ (as opposed to $\Sigma \approx 77L^2/(4\pi)$ for sCDM). Even in the presence of noise, wherever the signal dominates, the detection is better

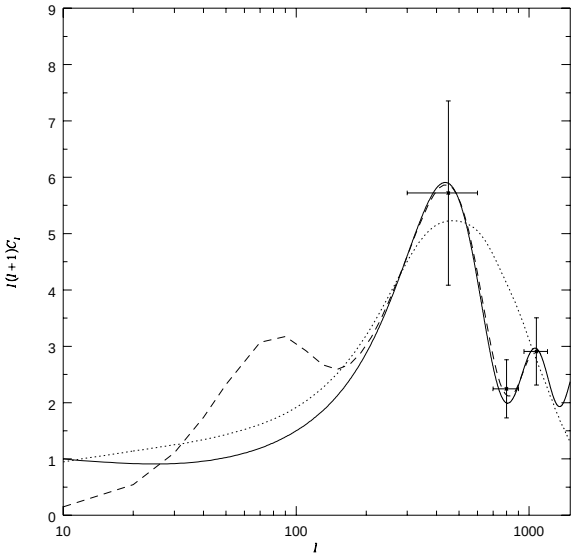

Figure 3: The angular power spectrum of stCDM (solid line) and one possible cosmic string scenario (dotted line). The dashed line is the ensemble average stCDM power spectrum as sampled by an experiment with a field size $L = 2$. The points indicate the average power in each bin for stCDM. The horizontal errorbars denote the width of the bins, and the vertical errorbars show the sample variance of the power estimates for such an experiment assuming no instrumental noise.

for stCDM. However, in noise-dominated regions the behaviour of the detection function for stCDM and CDM is very different.

The signal-dominated region is greatly reduced in stCDM. Much smaller beamsizes θ_b are now required for any meaningful detection. As shown in Fig. 4, one would now need $\theta_b < 0.3^\circ$ and $\theta_b < 0.25^\circ$, for noises $w^{-1} = (25\mu K)^2(\mathrm{deg})^2$ and $w^{-1} = (60\mu K)^2(\mathrm{deg})^2$ respectively, in order to obtain a reasonable detection. Again one can plot an ideal scanning line in the beam/coverage sections defined by a fixed noise w^{-1}. The ideal sky coverage is much smaller for stCDM than for sCDM. In general the contours of Σ for stCDM compared to sCDM are squashed to lower θ_b, lower L, and achieve higher significance levels, with steeper slopes. Following an ideal scanning line for any fixed w^{-1} one reaches a maximal detection allowed by the given level of noise, which is always better for stCDM than for sCDM. This maximal detection is normally obtained with a small sky coverage, and infinite resolution. Nevertheless, one falls short of this maximum by only a few sigma if the resolution is about $\theta_b = 0.05^\circ - 0.1^\circ$. From Fig. 4, for $w^{-1} = (25\mu K)^2(\mathrm{deg})^2$, one may now obtain a maximal 43-sigma detection for an ideal scanning area of $L = 65$ degrees. If $\theta_b = 0.1^\circ$ a 36-sigma detection is still obtained. We also see that a beamsize of $\theta_b < 0.25^\circ$ is required to obtain a 3-sigma detection (with $L = 4$ degrees), and a 10-sigma detection can be achieved only with $\theta_b \approx 0.15^\circ$ (and $L_i = 18$ degrees). All-sky coverage for an experiment targeting stCDM is generally inadvisable, and it would only be optimal for the extremely low level of noise $w^{-1} < (11\mu K)^2(\mathrm{deg})^2$.

5 Conclusions

The results obtained here are useful for future CMBR projects in two different ways. Firstly they allow the choice of an ideal scanning strategy (choice of resolution and sky coverage) for

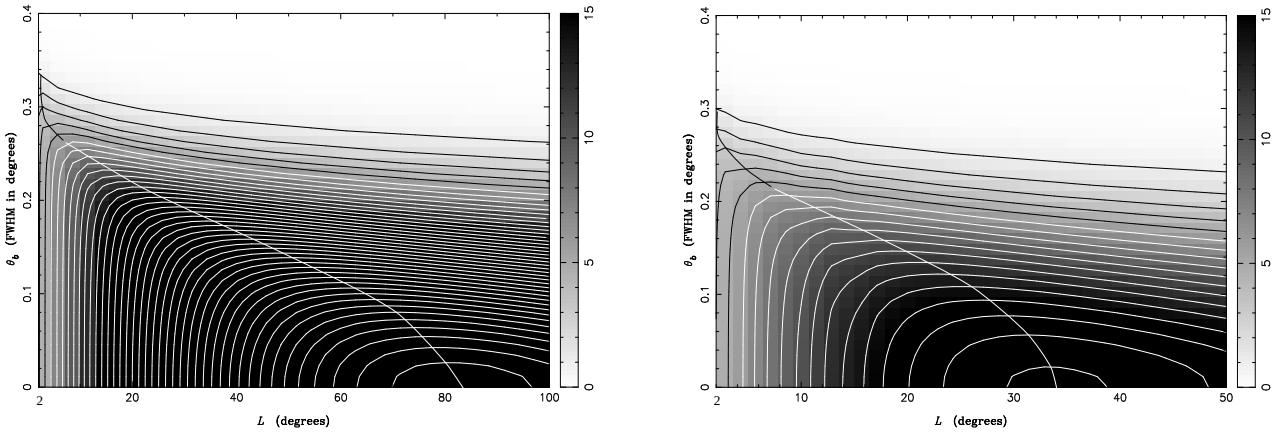

Figure 4: (Left) Low noise $w^{-1} = (25\mu K)^2(\text{deg})^2$ contours of the detection function Σ for stCDM. (Right) High noise $w^{-1} = (60\mu K)^2(\text{deg})^2$ contours of the detection function.

detecting secondary Doppler peaks, given observational constraints such as the instrumental noise level and the total observing time. Secondly, one may compute the expected value of the detection, assuming ideal scanning, as a function of these parameters. This provides lower bounds on experimental conditions for a meaningful detection as well as an estimate of how fast detections will improve thereafter.

These results also indicate that in order to study Doppler peak features for sCDM, depending on the noise levels, a large sky coverage might be desirable, even for a resolution of about $\theta_b = 0.4^\circ - 0.5^\circ$. If, however, one is instead to test the high-l opposition between low Ω CDM and cosmic strings, then a rather higher resolution is required. Furthermore, in this context, all-sky scanning is not only unnecessary, but in fact undesirable.

Acknowledgements. Thanks to Joao Magueijo for many useful discussions.

References

[1] Jungman G., Kamionkowski M., Kosowsky A., Spergel D., 1996, Phys. Rev. Lett., submitted.

[2] Albrecht A., Coulson D., Ferreira P., Magueijo J., 1996, Phys.Rev.Lett., 76, 1413

[3] Magueijo J., Albrecht A., Coulson D., Ferreira P., 1996, Phys.Rev.Lett., in press

[4] Crittenden R., Turok N., 1995, Phys. Rev. Lett., 75, 2642

[5] Durrer R., Gangui A., Sakellariadou M., 1996, Phys. Rev. Lett., 76, 579

[6] Tegmark M., Efstathiou G., 1996, *MNRAS*, in press

[7] Maisinger K., Hobson M. P., Lasenby A., 1996, *MNRAS*, submitted

[8] Becker R. H., White R. L., Helfand D. J., 1995, *Astrophys. J.* **450**, 559

[9] Hobson M. P., Mageuijo J.,1996, *MNRAS*, submitted

[10] Magueijo J., Hobson M. P., 1996, Phys.Rev.Lett., submitted